Positive antiphase boundary domain wall magnetoresistance in Fe_3O_4 (110) heteroepitaxial films

R. G. S. Sofin,* S. K. Arora, and I. V. Shvets

Centre for Research on Adaptive Nanostructures and Nanodevices (CRANN), School of Physics, Trinity College Dublin, Dublin 2, Ireland

(Received 20 July 2010; revised manuscript received 21 December 2010; published 27 April 2011)

We observe a strong crystallographic direction dependence on the low-field magnetoresistance (MR) behavior of the epitaxial Fe_3O_4 (110) films grown on MgO (110) substrates. The sign of MR is positive when the current and field are parallel to [001], whereas along the [$\bar{1}$10] direction its sign is negative, similarly to that commonly observed for (100) oriented Fe_3O_4 films. We relate this effect to the presence of antiphase boundaries (APB) and subsequent reduction in the width of canted spin structure in its vicinity, due to the hard axis behavior of Fe_3O_4 (110) films along this crystallographic direction. At fields greater than the anisotropy field, usual negative MR behavior related to a reduction in spin scattering at the APBs is observed. An analytical model based on the half-infinite spin chains across the APBs is provided to show that the positive MR is due to the domain walls along APBs. The temperature and film thickness dependency of the APB domain wall magnetoresistance is discussed.

DOI: 10.1103/PhysRevB.83.134436 PACS number(s): 75.70.Kw, 75.30.Gw, 75.47.Lx, 68.55.−a

I. INTRODUCTION

Electronic properties of domain walls (DWs) in ferromagnetic materials may differ from those of ferromagnetic domains.[1,2] A DW is an interface between uniformly magnetized regions (domains) with different magnetization directions. The length scale over which the magnetization direction changes is determined by material parameters such as the exchange and magnetic anisotropy energies.[1,2] The electrical resistance due to magnetic domain walls in metallic ferromagnets has received considerable attention for a long time.[1–5] Research activity in this area has increased substantially in the recent past due to the advances in material preparation and various nanofabrication techniques which allow one to control the DW dimensions and their number.[6–9] The origin of the DW resistance (DWR) in ferromagnetic metals is attributed to the mixing of up- and down-spin electrons due to the spin mistracking of the electrons on passing through the DW.[3] However, the models proposed for the ferromagnetic metals cannot be applied generally; for example, it is not sufficient to explain the DWR observed in itinerant ferromagnets such as $SrRuO_3$.[10] In thin films the resistivity contribution of DW is usually masked by various intrinsic and extrinsic factors such as anisotropic magnetoresistance (AMR), ordinary magnetoresistance (OMR), spin scattering related to magnetic in-homogeneities, and so on.

In recent years a lot of attention has been given to the studies of the structural, magnetic, and magnetotransport properties of heteroepitaxial thin film structures based on magnetite (Fe_3O_4) thin films, which is a very good example of a strongly correlated half-metal with significant polaronic effects.[11–20] The interest is partly due to the great application potential of this material in spintronics. Fe_3O_4 is one of the most important half-metallic oxides with the highest Curie temperature ($T_C = 858$ K).[21] There are many reports on the growth of Fe_3O_4 thin films on different types of substrates like MgO, $MgAl_2O_4$, sapphire, Si, or GaAs using a variety of deposition techniques.[11,12,22–27] MgO (lattice constant 0.4212 nm), which has a rock salt crystal structure, is a widely used substrate for epitaxy of magnetite (lattice constant 0.83987 nm) due to the small lattice mismatch of only 0.33%.[9] Antiphase boundaries (APB) are structural defects occurring in thin films during epitaxial growth and are observed in Fe_3O_4 films when grown on a variety of substrates like MgO, $MgAl_2O_4$, and α-Al_2O_3.[11,12,28–30] Since the Fe_3O_4 ($Fd\bar{3}m$) crystal structure is of lower symmetry than MgO ($Fm3m$), there are several equivalent nucleation sites on the MgO (100) surface, which enforce the formation of APBs at the interface of the neighboring grains. An atomic step in the MgO substrate can also lead to the formation of APB in Fe_3O_4 since the lattice constant of Fe_3O_4 is almost exactly double that of MgO.[31] The presence of APBs leads to a large difference between the physical properties of epitaxial Fe_3O_4 films and those of the bulk such as larger electrical resistivity,[28] magnetoresistance,[32] and magnetization which does not saturate in high magnetic fields.[33]

The APBs, which can be envisaged as the disruption of cation chains in a continuous oxygen lattice, lead to new magnetic exchange interactions, which are not present in the bulk material.[28] There are many possible types of APBs, each characterized by its own type of atomic coordination and consequently its own type of exchange interactions. Exchange interactions occurring across some of the APBs must be antiferromagnetic (AF), and experimental evidence suggests that these AF-APBs dominate the magnetic and magnetotransport properties of Fe_3O_4 thin films.[20,32,34] It was shown that if the spins on neighboring ions are not parallel but, instead, form an angle φ_{nn}, the transfer integral is reduced to$t = t_o \cos \varphi_{nn}/2$.[32] Therefore, the transfer of the conduction electrons between ions with antiparallel spins at an AF-coupled APB is blocked and, according to the model, the conductivity reduces to zero. The conductivity becomes finite if the angle deviates from π by the application of a magnetic field.[32] This explains the observation of negative magnetoresistance in Fe_3O_4 thin films grown on MgO substrates. The resistivity contributions from AMR, domain wall magnetoresistance (DWMR), OMR, and so on, are expected to be negligible when compared to the much greater resistivity contribution from AF-APBs in Fe_3O_4 thin films. In the case of thin films, due to easy plane shape anisotropy, the spins far from APBs lie in plane and

at the boundary, and the AF-coupled spins lie out of plane, forming a domain wall across APB which is distinct from the usual 180° walls due to the abruptness of the AF coupling at the boundary.[32] Studies on 25-nm-thick Fe_3O_4 (100) film using dark-field transmission electron microscopy (TEM) and off-axis electron holography reveal that a large proportion of APBs have out-of-plane moments at the boundary which rotate to an in-plane orientation over a distance of approximately 15 to 20 nm.[35] Apart from the misalignment of spins in the vicinity of APB due to strongly coupled AF spins across the boundary leading to contribution to MR, the magnetic domain walls formed along the APB (APB-DW) can also contribute to the resistivity. These APB-DW are expected to have widths smaller than conventional ones due to AF exchange at the APB. Thus it could make much greater contribution to DWMR compared to conventional DW. This contribution would be noticeable only at applied field values where the negative resistivity contribution due to the rotation of AF-coupled spins at the APB is small. It was also shown that the coarse magnetic domains are 5 to 14 times greater than the APB domains.[35] Therefore, the density of the APB domain walls is much greater compared to that of conventional magnetic domain walls. In this paper, we present the results of MR studies on Fe_3O_4 (110) films with different thicknesses grown on MgO (110) substrates. These films show substantial in-plane magnetic anisotropy and anomalies in the characteristic behavior of MR when measured along the [001] direction. A positive longitudinal MR is observed at low fields when current and magnetic field are directed along the [001] hard magnetization axis and a typical negative MR curve is observed when measured along [$\bar{1}$10]. With an analytical model of half-infinite spin chains, we show that the occurrence of this positive MR at low fields is due to APB-DW ($DWMR_{APB}$). To the best of our knowledge there are no reports on the crystallographic direction dependence on MR properties of Fe_3O_4 (110) films.

II. EXPERIMENTAL METHOD

The Fe_3O_4 thin films (thicknesses of 30, 60, and 90 nm) were grown on (110)-oriented MgO single crystal substrates (cut along the [110] direction within ±0.5°) using an oxygen plasma–assisted molecular beam epitaxy (MBE) system (DCA MBE M600) with a base pressure of 2×10^{-10} Torr. The substrates were annealed *in situ* at 600°C in 5×10^{-6} Torr oxygen for 2 h. Growth of the Fe_3O_4 films was carried out at a substrate temperature of 250°C from a pure metallic Fe source by means of electron beam evaporation and oxygen free radicals generated by the electron cyclotron resonance (ECR) plasma source. The plasma source was operated at a power of 80 W in an oxygen partial pressure of 1×10^{-5} Torr. Reflection high-energy electron diffraction (RHEED) (STAIB Instruments) was used to monitor the growth mode and growth rate. After the cleaning procedure, the RHEED pattern of the MgO (110) single crystalline substrate measured along the [001] and [$\bar{1}$10] azimuths, respectively, showed vertical lattice rods and radial Kikuchi lines indicative of a well-ordered and flat surface. The RHEED pattern after the film growth showed half-order streaks and was accompanied by the oscillations in the intensity of specularly reflected beam. The period of oscillation corresponds to the growth rate 0.3 Å/s and confirms that the film growth occurs in a layer-by-layer mode. Auger electron spectroscopy (AES) studies and high-resolution TEM imagery (close to the atomic resolution) on Fe_3O_4 (100) [grown on MgO(100) substrates using same MBE setup and annealing conditions] showed that there is no signature of Mg or other impurities in these films or interfaces.[11,12,16] X-ray reflectivity measurements on the films showed thickness of 30, 60, and 90 nm (±2 nm). The thickness values determined from reflectivity measurements are in good agreement with the thickness estimated from observed growth rate from RHEED intensity oscillations.

Magnetization measurements were performed using an alternating gradient-field magnetometer (Micromag-3900, Princeton Measurements, USA) with a sensitivity of 10^{-8} emu. The magnetization versus field (M-H) loops were measured at room temperature by applying the magnetic field (maximum field of 1 T) in the film plane along the [001] direction and [$\bar{1}$10] directions. The diamagnetic contribution from the MgO substrate was subtracted from the measured data by performing an M-H loop in the same field range of the MgO substrate of similar dimensions as that of thin film samples.

Structural characterization of the films was done using a multicrystal high-resolution x-ray diffractometer, HRXRD (Bede-D1, Bede, UK). The HRXRD (wavelength = 0.154056 nm corresponding to **a** Cu K-α line) in a double or triple axis configuration was performed to confirm the epitaxial relationship of the Fe_3O_4/MgO heteroepitaxy. The out-of-plane ($a_\perp$) lattice parameter was determined from the analysis of ω-2θ scans measured around the symmetric (220) diffraction planes common to the substrate and thin film. The in-plane lattice constant $a_{||} = d_{001}$, was measured by performing asymmetric scans on {222} and {444} diffraction planes of the substrate and thin film. In the case of a tetragonally distorted epilayer (e.g., Fe_3O_4/MgO) the asymmetric diffraction plane is tilted with respect to the equivalent asymmetric diffraction plane in the substrate. This difference in inter planar angle is denoted by $\Delta\Phi$. Thus a convenient method for canceling out the effect of $\Delta\Phi$ is to take measurements of both the (*h k l*) (gracing exit geometry, GE) and (*-h-k l*) (gracing incidence geometry, GI) planes.[11,12] This method is very effective for the precise determination of in-plane lattice parameter of thin films by removing any errors due to strain tilt. The estimated x-ray probing depth for 90% contribution of the measured intensity at GI angle of 3.969° (Fe_3O_4{444} peak) is 834 nm, which is well above the thickness of the samples used in these studies.

For electrical resistivity and magnetoresistance measurements a standard dc four-probe technique was employed. The sample was mounted on a copper block fitted onto a cold finger of a closed cycle refrigerator. Temperature of the sample stage was monitored using a GaAlAs thermometer and controlled within ±0.05 K. For magnetotransport measurements, the cold finger was inserted into an electromagnet with a maximum field of 1 T (Bruker, Germany, Model:B-E10V). The magnetoresistance results reported here were obtained by keeping the direction of magnetic field and current parallel to each other unless otherwise stated. The MR is defined as MR% = [*R*(*H*)-*R*(0)/*R*(0)] × 100, where *R*(*H*) and *R*(0)

are the resistances of the sample with and without field, respectively.

III. RESULTS

Figure 1 shows the ω-2θ scans (measured in triple-axis configuration at room temperature) for the (220) and (440) symmetric Bragg reflections of MgO and film, respectively, for all three samples. The horizontal axis in the figure is shown with reference to the Bragg angle of the (220) reflection for MgO substrate. The curves are shifted along the vertical axis for clarity. The full width at half of maximum (FWHM) of the film peak was found to decrease with increasing film thickness. The FWHM for the film peak was found to be 0.19°, 0.09°, and 0.06° for 30–, 60–, and 90-nm-thick films, respectively. The value of $a_\perp$ for the Fe_3O_4 thin films was determined from the separation of film-substrate peaks and was found to increase with increasing film thickness. From the analysis of grazing exit and grazing incidence asymmetric scans on {222/444} set of planes [shown in Figs. 2(a) and 2(b)], we obtained the in-mr lattice parameter of the films. The out-of-plane and in-plane lattice constants are shown in the Table I. The in-plane lattice constant along [001] was found to be decreasing and approaching toward the bulk value for 60- and 90-nm films. The detailed structural characterization shows that the films undergo strain relaxation above 30-nm film thickness and the amount of strain reduces (but not canceled) with increasing film thickness with increasing thickness. The observed strain is 0.345, 0.342, and 0.335% for 30-, 60-, and 90-nm films respectively. Figure 3 shows resistivity as a function temperature for various thicknesses. The resistivity of the films is found to be thickness dependent. The magnitude of resistivity increases with a decrease of film thickness. The onset value of Verwey transition temperature (T_V) for these films was found to be thickness dependent (108 K, 109 K, and 110.6 K (±0.1 K) for 30-, 60-, and 90-nm films, respectively). Since the Verwey transition is very sensitive to the Fe_3O_4 film stoichiometry,[36] the presence of the Verwey transition confirms the high quality of the films. The lower value of T_V in thin films compared to bulk (∼125 K) could be to the reticence of long-range order of the Fe^{2+} and Fe^{3+} ions at the octahedral sites, which is necessary for the Verwey transition, caused by small APB domain sizes.[28,30,37] These findings for the thickness-dependent behavior of resistivity and Verwey transition temperature are consistent with earlier transport studies on Fe_3O_4/MgO (100) heteroepitaxial system.[38]

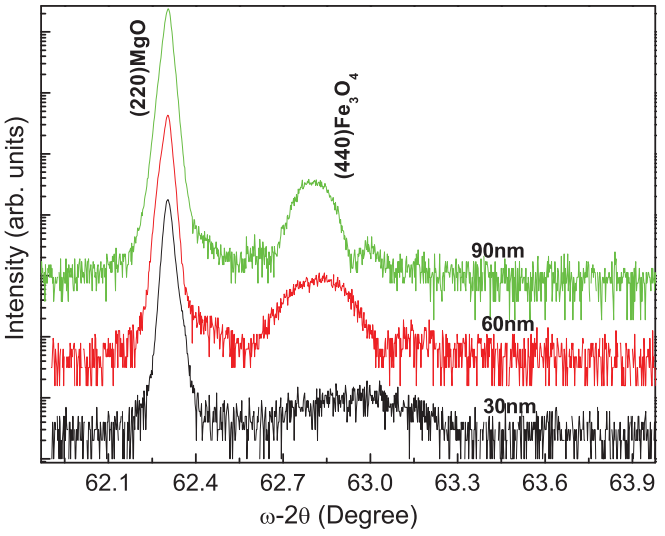

FIG. 1. (Color online) The ω-2θ scans for Fe_3O_4 films with different thickness on MgO (110) substrates, measured for symmetric (220) Bragg reflection common to substrate and thin film. Curves are shifted along the vertical axis for clarity.

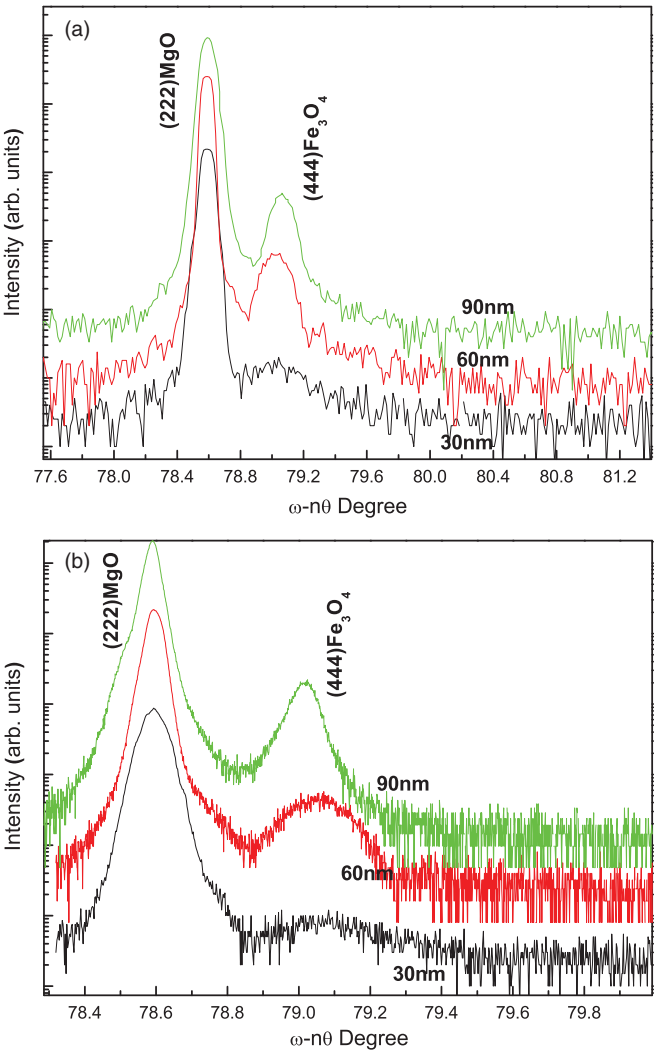

FIG. 2. (Color online) The ω-$n\theta$ scans for Fe_3O_4 films with different thickness on MgO (110) substrates, measured for asymmetric {222} Bragg reflection in (a) grazing exit and (b) grazing incidence common to substrate and thin film. Curves are shifted along the vertical axis for clarity.

TABLE I. Out-of-plane and in-plane lattice constant of films with various thicknesses.

Thickness (nm)	$a_\perp$ Å (±10^{-4} Å)	$a_{\|\|}$ Å (±10^{-4} Å)
30	8.3833	8.4223
60	8.3943	8.4258
90	8.3952	8.4252

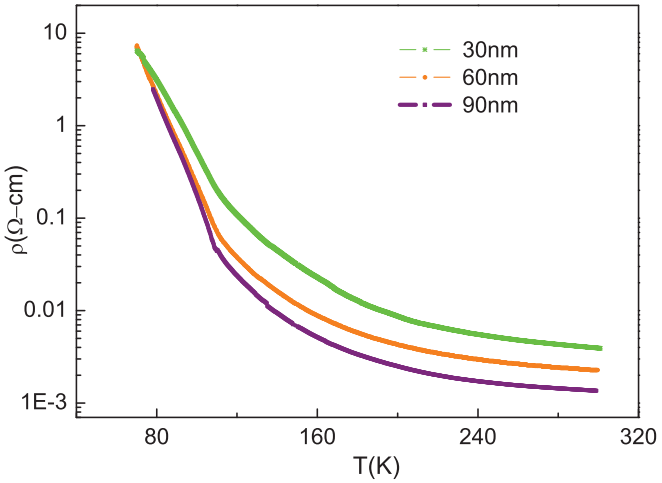

FIG. 3. (Color online) Resistivity of films with thicknesses 30, 60, and 90 nm as a function of temperature.

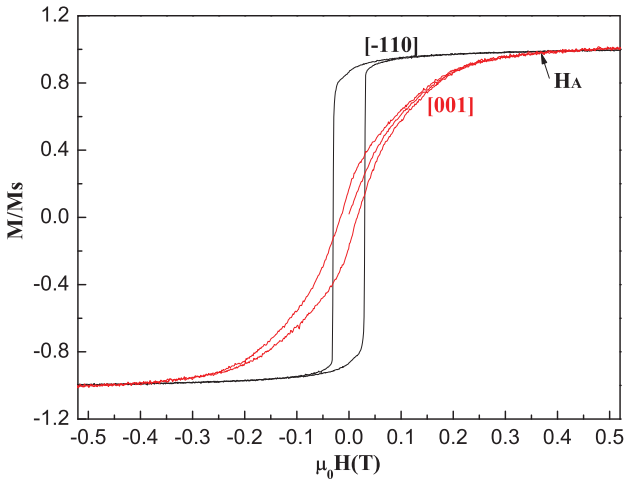

FIG. 4. (Color online) Hysteresis loops obtained for 90-nm Fe_3O_4 (110) film measured at 300 K with an in-plane field directed along either the [$\bar{1}$10] or [001] direction.

Figures 4 show hysteresis loops obtained at room temperature for a 90-nm film measured at 300 K with an in-plane magnetic field aligned in [$\bar{1}$10] and [001] directions respectively (magnetization is normalized with saturation magnetization, M_s). The hysteresis loops obtained at 300 K in [$\bar{1}$10] is nearly square ($M_r/M_s = 0.86$) and in the [001] direction it shows hard axis behavior. All our films showed a similar behavior. Although bulk magnetite has a cubic anisotropy with a ⟨111⟩ easy axis, reports on magnetization studies of Fe_3O_4 (110) epitaxial films grown on MgO (110) substrates show a square hysteresis loop with an in-plane [$\bar{1}$10] easy axis and [001] hard axis, consistent with our measurements.[39] Low-temperature magnetization measurements show a clear transition from hard axis to easy axis behavior below the Verwey transition when measured along [001] direction. It is well known that certain crystallographic directions can be made magnetically soft below transition by cooling the crystal through the transition with a magnetic field applied in these directions.[40] A discussion pertaining to this issue is outside the scope of this article.

The magnetization curves can be analyzed using a simplified equation, $M(\mu_0 H)/M(\infty) = 1 - qH^{-0.5}$, described in Ref. 34. The parameter q measures the difficulty of approaching saturation. The virgin magnetization curves [normalized by $M(\mu_0 H = 1$ T)] measured along [001] at room temperature were fitted using the above equation and the values of q obtained for 30-, 60-, and 90-nm films were 0.22, 0.16, and 0.097 ± 10^{-4} $T^{0.5}$, respectively. Corresponding values obtained along [$\bar{1}$10] were 0.056, 0.047, and 0.025 ± 10^{-4} $T^{0.5}$ which are an order of magnitude less compared to the [001] direction. However, the values of the exponents for a power law fit to the thickness dependency of q were -0.71 and -0.7 ± 10^{-2} along [001] and [$\bar{1}$10], respectively. The above analysis and the observation of similar values of the exponents along the two directions suggests that the parameter b depends on APB domain size (which is thickness dependent) and the size evolution of APB domains are isotropic. The values of q (measured along [001]) are of the same order but higher compared to the values reported for Fe_3O_4 (111) and Fe_3O_4 (100) films of comparable thicknesses grown on α-Al_2O_3 and MgO substrates respectively.[34,41] This could be because of the differences in the APB network geometry, the fraction of APBs exhibiting AF couplings, and the difference in the APB density.

Field dependency of MR shows drastically different features when measured along [001] direction as compared to [$\bar{1}$10] direction. Figure 5 shows the MR at different temperatures for 90-nm film with field and current directed along the [001] direction. Above T_V, films showed symmetric butterfly-shaped positive MR at low field while MR along [$\bar{1}$10] direction shows negative MR characteristics similar to the MR (with in-plane field) measured on (100) Fe_3O_4 films (see Fig. 5). At high fields MR along [001] was found to be negative and it increases with decrease in temperature for all the films and peaks near T_V. Figure 6 shows the MR values in a 0.9-T field as a function of temperature for all three samples. Below T_V the magnitude of high-field MR

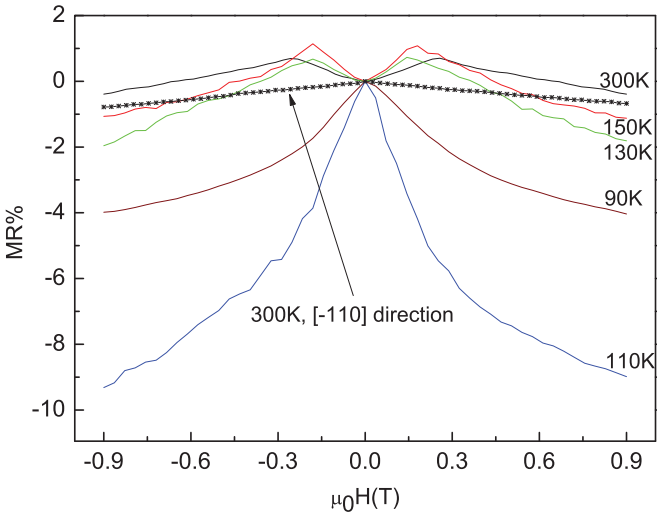

FIG. 5. (Color online) Magnetoresistance measured at different temperatures for a 90 nm film with an in-plane field and current directed along the [001] direction. Magnetoresistance measured in the [$\bar{1}$10] direction at 300 K is also shown.

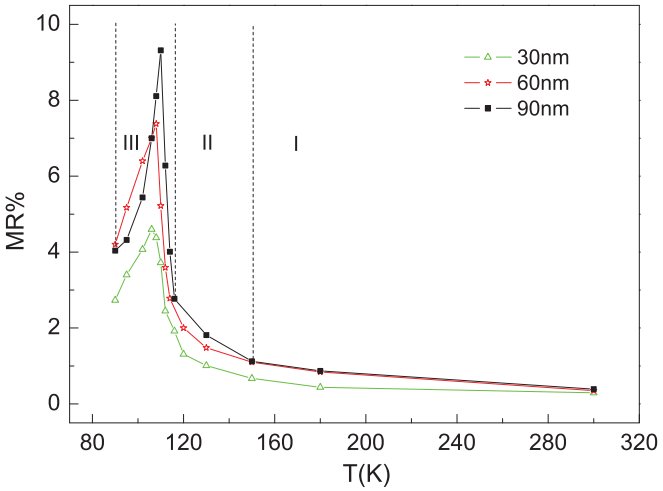

FIG. 6. (Color online) Magnetoresistance as a function of temperature for films having different thickness at 0.9-T field. Magnetic field and current directed along the [001] direction. Different temperature domain areas are marked as I, II, and III.

along [001] was higher compared to the $[\bar{1}10]$ direction (5% difference at T_V and 1-T field) and MR measured (irrespective of the measurement direction) in (100)-oriented films (2%-3% difference at T_V and 1-T field).[31] Figure 7 shows the maximum value of positive MR as a function of temperature for various film thicknesses. As temperature is lowered positive MR peaks at a temperature T_p ($T_p \sim 116$ K, 130 K, and 150 K for 30, 60, and 90 nm, respectively) and vanishes near T_V. As explained in the following discussion we attribute this positive MR to APB-DWMR.

IV. DISCUSSION

In order to understand the observed positive MR, we consider various known sources of MR. A classical positive MR which arises in a two-band model from the action of the Lorentz force on the carriers is generally called OMR.

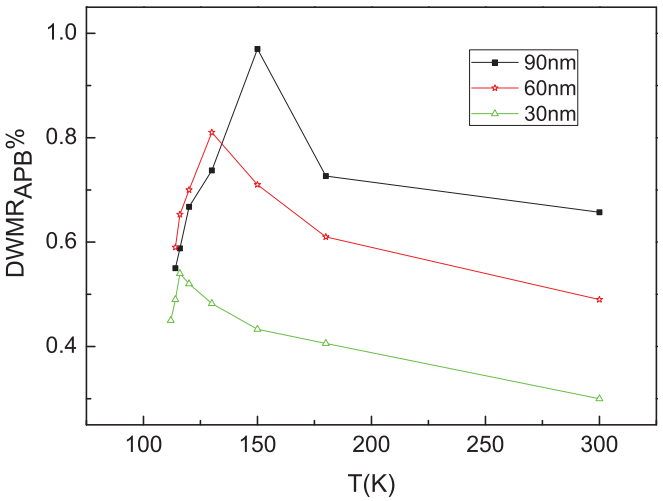

FIG. 7. (Color online) $DWMR_{APB}$ of epitaxial Fe_3O_4 films measured along the [001] direction as a function of temperature for films having different thicknesses.

The Lorentz force–related contribution can be observed if $\omega_c\tau > 0.1$, where ω_c is the cyclotron frequency, $\omega_c = \frac{eB}{mc}$, and τ is the scattering time. For magnetite films it was shown that $\omega_c\tau \sim 10^{-5}$ and, therefore, Lorentz force effects can be ruled out.[19] Another source of the positive MR could be related to the anisotropic magnetoresistance (AMR), which is caused by the spin-orbit interaction.[23] AMR is defined as $[\frac{\Delta\rho}{\rho}]_{\parallel-\perp} = \frac{\rho_\parallel - \rho_\perp}{\rho_{ave}}$, where $\rho_{ave} = \frac{\rho_\parallel}{3} + \frac{2\rho_\perp}{3}$, $\rho_{||}$ and $\rho_\perp$ denote the longitudinal ($M \parallel j$) and transverse ($M \perp j$) resistivities, respectively. In the case of magnetite films these resistivities decreases with field and provide only a negative contribution to MR.[19,23]

To explain the negative MR observed in Fe_3O_4(100) films grown on MgO(100) substrates, Eerenstein *et al.* have used a model which considers two spin chains separated by an AF-APB.[32] Ramos *et al.* have used an extended version of the model given by Eerenstein *et al.* to validate the longitudinal MR data of Fe_3O_4 (111) films grown on α-Al_2O_3 substrate, observed in the high-field regime.[29,32] To understand and explain the spin transport in Fe_3O_4 (110) films, in particular the positive MR along the [001] direction, we consider a model similar to Ref. 32 as the APBs are expected to form in the case of Fe_3O_4 films grown on MgO (110) substrates as well (please see the Appendix for details). Our model takes into account an in-plane anisotropy energy density term that manifests through modification in spin transfer behavior along different crystallographic directions. All the previous reports focus on the scattering of spin polarized electrons at the AF APBs.[29,32] The significant difference in our analysis is that we discuss the scenario where a positive resistivity contribution occurs due to the tapered spin chains near the boundary in addition to the scattering due to AF spins at the boundary. Prior to discussing the details of the model, we would like to mention that there is a significant difference in the strength of magnetocrystalline anisotropy between the Fe_3O_4(100) films and the Fe_3O_4(110) films, its strength being greater for the latter case. Let us consider a half-infinite spin chain on one side of the APB. In the direct vicinity of APB, the spins are misaligned due to frustration of exchange interaction at the APB. At some distance λ away from APB, the effect of the exchange frustration vanishes and the spins are almost aligned either along the external field H or along the easy axis of magnetocrystalline anisotropy. Whether it is aligned along H or the easy axis depends on the direction of the field and its strength. For example, if the field is aligned along the hard axis, then at a low-field value, the spins are aligned approximately along the easy axis and at high field ($H > H_A$) they are aligned along the field. We can consider two cases here. A spin chain with field applied along [001] direction (case a) and along $[\bar{1}10]$ direction (case b). In case a we can write the energy per unit area of a half-chain as

$$\gamma_{001}(\varphi_o, H) = \int_{-\lambda}^{o} \left[M_s H(1-\cos\varphi) + K\left(\frac{1}{4}\sin^4\varphi + \sin^2\varphi\cos^2\varphi\right) + A_F\left(\frac{d\varphi}{dx}\right)^2 \right] dx, \quad (1)$$

where φ is the angle between local magnetization and field H and λ is the distance from the APB at which spins are

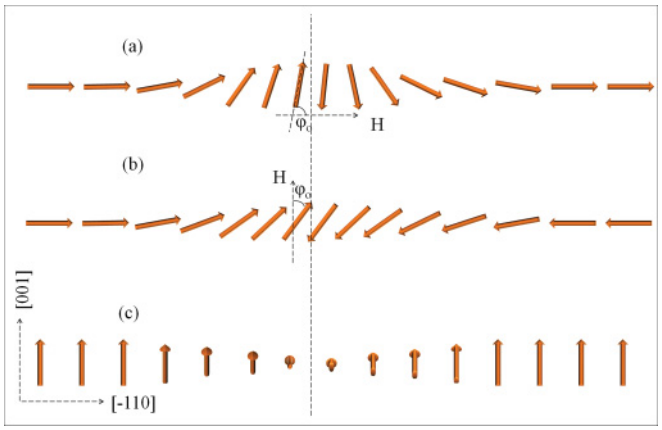

FIG. 8. (Color online) Various spin configurations with applied field (a) field along [-110] direction (b) field along [001] below anisotropy field (c) field along [001] above anisotropy field.

aligned either along the field or the easy axis. The first term in the integral is the Zeeman and the second term is the cubic anisotropy energy density. The third term is the exchange energy density. K is the magnetocrystalline anisotropy constant and A_F is the exchange stiffness constant. The shape anisotropy of demagnetizing field is not relevant here, as in both cases the field is directed in the film plane. With variational calculus the condition for minimum energy can be derived as

$$M_s H\sin\varphi + K\cos\varphi\sin\varphi(3\cos^2\varphi - 1) = -2A_F\left(\frac{d^2\varphi}{dx^2}\right), \quad (2)$$

which states that torque is zero everywhere along the spin chain. When the field is zero, the spins far from the APB will be aligned in the easy axis direction and with increasing field they will gradually rotate toward the direction of the field. Now we can further consider two situations here, where the applied field is above and below the magnetocrsytalline anisotropic field H_A. Above H_A, the spins far from the APB will be aligned with the in-plane field while AF-coupled spin near APB will make an angle $\varphi_o$with the field [see Figs. 8(a) and 8(c)]. Below H_A spins far from the APB orient approximately in the easy axis directions ($\langle\bar{1}10\rangle$) and spin near APB makes an angle φ_o with the field [see Fig. 8(b)].

With these conditions, from Eq. (2) we can show that, for the case of H parallel to [001], when $H < H_A$

$$\sqrt{A_F}\left(\frac{d\varphi}{dx}\right) = \left[-M_s H\cos\varphi_o - \frac{K}{32}(1 + 4\cos2\varphi_o + 3\cos4\varphi_o)\right]^{\frac{1}{2}} \quad (3)$$

$$\frac{d\gamma}{d\varphi} = 2\sqrt{A_F}\left[-M_s H\cos\varphi_o - \frac{K}{32}(24\cos^4\varphi_o - 16\cos^2\varphi_o)\right]^{\frac{1}{2}} \quad (4)$$

and when $H > H_A$

$$\sqrt{A_F}\left(\frac{d\varphi}{dx}\right) = \left[M_s H(1 - \cos\varphi_o) + \frac{K}{32}(7 - 4\cos2\varphi_o - 3\cos4\varphi_o)\right]^{\frac{1}{2}} \quad (5)$$

$$\frac{d\gamma}{d\varphi} = 2\sqrt{KA_F}\left[\frac{M_s H}{K}(1 - \cos\varphi_o) + \frac{1}{32}(7 - 4\cos2\varphi_o - 3\cos4\varphi_o)\right]^{\frac{1}{2}}. \quad (6)$$

Now considering the spin chains on both sides of the APB with an angle $\varphi_o = \varphi_1$ and $\varphi_o = \varphi_2$ for the left and right side chains, the energy density of antiferromangnetic coupling at the boundary can be written as[32]

$$\gamma_{\mathrm{AF-APB}} = \frac{A_{\mathrm{AF}}}{d}(1 - \cos(\varphi_2 - \varphi_1)), \quad (7)$$

where A_{AF} is the negative exchange stiffness constant for the AF exchange interaction at the boundary and d is the distance between the neighboring chains along the boundary. The final approximate result of minimization is $\varphi_1 = -\varphi_2 = \frac{\varphi_{\mathrm{nn}}}{2} = \varphi_{\mathrm{AF}}$ and

$$\cos^2\varphi_{\mathrm{AF}} = \frac{(M_S H)^2}{K(W - 2\sqrt{2KW + K})} \quad H < H_A, \quad (8)$$

$$\cos^2\varphi_{\mathrm{AF}} = \frac{(4M_S H + K)}{(4W - 12K)} \quad H < H_A, \quad (9)$$

where $W = A_{\mathrm{AF}}^2/A_F d^2$.

The dc conductivity in Fe_3O_4 can be explained by the superposition of a small polaron band and hopping conduction.[42] It was shown that in the nonadiabatic limit the conductivity $\sigma \propto t^2$, where the transfer integral t can be expressed as $t^2 = t_o^2\cos^2\varphi_{\mathrm{AF}}$.[32,42] Eerenstein *et al.* have shown that MR $= -\cos^2\varphi_{\mathrm{AF}}C$, where C is a constant which depends on the volume fraction of the APB domains.[32] From Eq. (8), it is evident that for a field below the anisotropy field, H_A, the conductivity across the antiferromagnetically coupled APB will decrease quadratically (small change) with the field and is linear (large change) above H_A. Therefore in the low-field regime the MR contribution from other factors should dominate over the MR contribution due to AF-APBs.

Similar analysis for case b, with the field along the easy axis [$\bar{1}$10] direction and an anisotropy energy density $\gamma_a = K[\frac{1}{4}\cos^2 2\varphi]$, gives

$$\cos^2\varphi_{\mathrm{AF}} = \left[\frac{M_s H}{W + K}\right], \quad (10)$$

which suggests that the field dependence of MR is linear only.

DWMR predicted by the Levy and Zhang (LZ) model for ferromagnetic metals is given by $\frac{\Delta\rho}{\rho} = \frac{\xi^2}{5}F(\alpha)$, where ξ is the spin mistracking parameter and is given by $\xi = \pi\hbar^2 k_F/4mwJ$, where $k_F$is the Fermi wave vector, m is the effective mass, J the Stoner exchange splitting, and w is the domain wall width. α is the spin asymmetry of the current.[3] For our case, we can take the essential predication of this model, which is DWMR $\propto \omega^{-2}$.

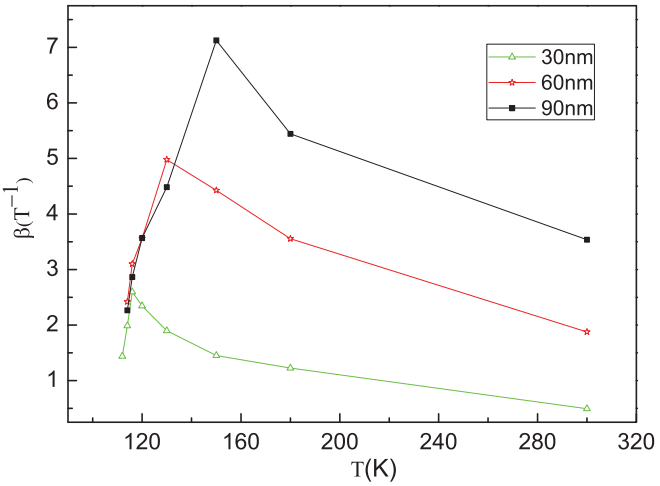

FIG. 9. (Color online) β as a function of temperature.

For the case of $\varphi_o = \pi$, from Eq. (3) we can deduce $\lambda \propto 1/\sqrt{H}$, which means the width of the canted spin chain λ reduces with increasing field. The same dependency of λ on H can be derived in the case where $H > H_A$ and in case b. But the essential difference between these two cases and the case where $H < H_A$ is that, as λ decreases with increasing field, the angle between the spins (within the distance λ) decreases in the former case while it increases in the latter case. This is due to the differences in the rotation of AF-coupled APB spins with the field as explained earlier. Therefore the formation of highly canted spin structure below H_A should contribute some resistance to the traversing spins. Considering the model of DWMR we can write $\text{DWMR}_{\text{APB}} \propto \frac{1}{\lambda^2} = \beta H$, where β is a constant. This additional positive MR is visible because of the low negative MR contribution from APBs at low-field values ($H < H_A$). Figure 9 shows the variation of β, which is extracted from the linear fit to the positive region of the MR curves of various film thicknesses with temperature. β follows the same trend of DWMR_{APB} shown in Fig. 7 which peaks at temperature T_p. In the case of negative MR as a function of temperature, we can identify three different regimes as shown in Fig. 6 (regimes I, II, and III are marked only for the 90-nm film for clarity). There is a clear change in the slope from regime I to regime II. These regimes are found to be thickness dependent and T_p observed in the case of DWMR_{APB} matches with the center of regime II. The difference between the spin-dependent transport mechanisms in these regions could be related to the peaking of DWMR_{APB} at T_p. Below T_V DWMR_{APB} vanishes. This is related to the hard axis to easy axis transition below T_V in the [001] direction. This will lead to a situation similar to the analysis of MR behavior along the $[\bar{1}10]$ direction, where MR is dominated by the APB contribution only.

DWMR_{APB} is found to increase with the film thickness. It was shown that the APB domain size D is proportional to $\sqrt{t}$, where, t is the film thickness.[28] Micro magnetic simulations reported by Bataille *et al*. show that APBs can no longer be considered independent when the distance between them is less than 40 nm and the blocking field H_B increases as film

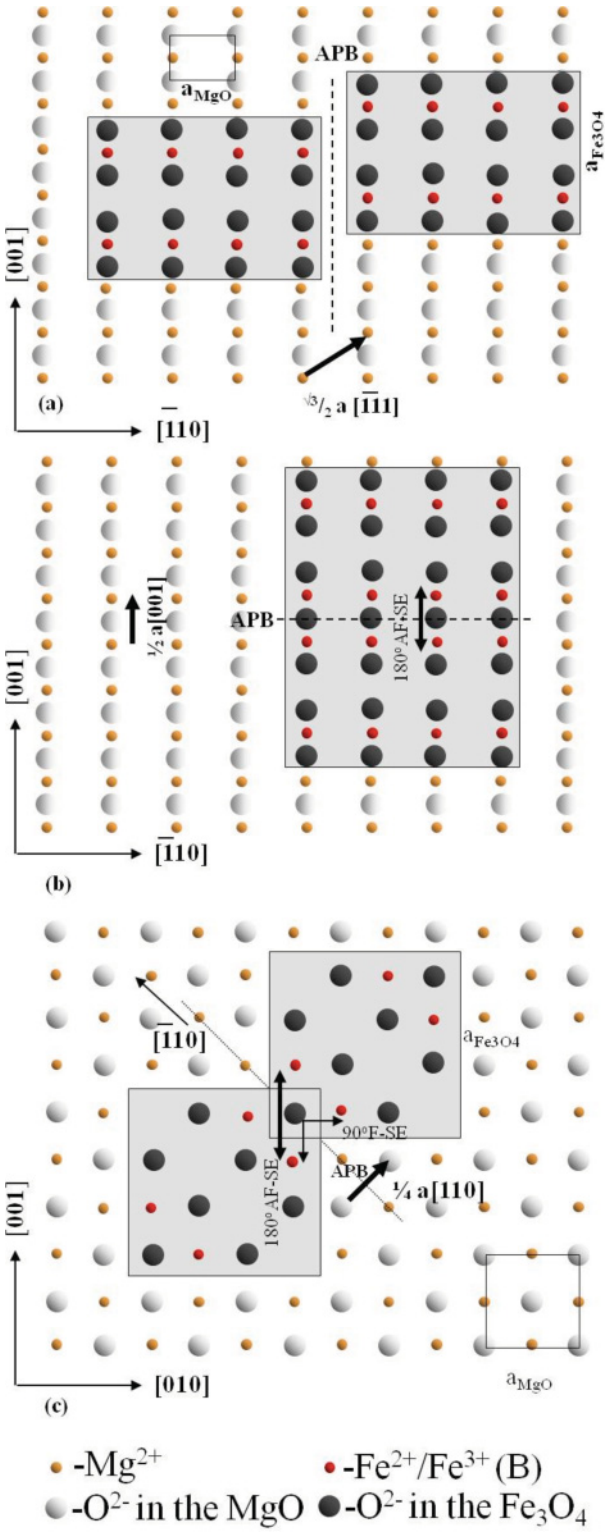

FIG. 10. (Color online) Schematic illustration of APB formation with (a) a $\sqrt{3/2}$ **a**$\langle\bar{1}11\rangle$ shift vector and (b) by a 1/2 **a** $\langle 001\rangle$ shift vector in (110)-oriented Fe_3O_4 films grown on MgO (110) substrates. Large square indicates unit cell of Fe_3O_4 (110) and small square indicates MgO (110) unit cell. (c) Formation of APB with shift vector 1/4 **a** $\langle 110\rangle$ on MgO (110) surface. [(b) and (c)] The possible antiferromagnetic and ferromagnetic super exchanges (SE) across APBs.

thickness decreases.[34] This is due to the reason that, when two AF-APBs come closer the spins within the boundary can be pinned, which allows for less rotational freedom compared to spins in larger domains. This could be the reason for the dependency of $DWMR_{APB}$ on film thickness. The field corresponding to maximum value of $DWMR_{APB}$ is found to be 0.26 T at room temperature (see Fig. 5). This value is almost near but smaller than the H_A (∼0.36 T) measured through magnetization measurements (see Fig. 4). This suggests that decoupling of the AF spins at the boundary starts at a field value lower than the anisotropy field and therefore negative MR starts to dominate. Eerenstein *et al*. have used a similar model to predict quadratic field dependence for the low-field MR, when field is applied perpendicular to the current and film plane of Fe_3O_4(100) films.[32,43] It is not possible to have a direct comparison of our model and results with theirs due to the following reasons. Fe_3O_4(100) epitaxial thin film has small in-plane anisotropy and therefore the modeling is done by considering only the uniaxial shape anisotropy.[32,43] In the Fe_3O_4 (110) thin film case there exists a strong in-plane anisotropy on top of the shape anisotropy. This suggests that the rotations of the spin chains in the applied field differ in these two cases. Another reason is the difference in the way Fe-O-Fe ions meet at the APBs in both these cases due to symmetry differences. For example, one such difference is depicted in Figs. 10(b) and 10(c). Here APB formation along the [-110] direction on (110)- and (100)-orientated MgO surfaces are compared. 10(b) relates to the (110) surface and shows a perfect 180° AF super exchange while Fig. 10(c) relates to the (100) surface and shows superposition of 180° AF and 90° ferromagnetic superexchanges. This superposition of two opposite types of exchanges in the latter case could reduce the AF coupling strength leading to the domination of negative MR and hindering the observation of positive $DWMR_{APB}$. The MR measurement configuration used by Eerenstein *et al*. differs from ours. What we measure is longitudinal magnetoresistance (where the current J and field H are parallel to each other) while their measurement is for transversal MR (where j is perpendicular to H), which again makes it difficult for a direct comparison. From the above analysis it is evident that positive MR observed is due to the $DWMR_{APB}$. Since the formation of APBs is not confined to a specific system like Fe_3O_4/MgO heteroepitaxy, the findings could be applied to other systems as well.

V. CONCLUSIONS

In conclusion we have performed detailed studies of structural and magnetotransport properties of Fe_3O_4 (110) films grown on MgO (110) substrate. Fe_3O_4(110) films show a significant in-plane magnetocrystalline anisotropy which is not present in Fe_3O_4(100) films grown on MgO (100) substrates. We found characteristic differences in the nature of MR between the longitudinal MR along [$\bar{1}$10] and [001] directions. Longitudinal MR along [001] is positive at fields below the magnetocrystalline anisotropy field. With an analytical model based on the half-infinite spin chains across APBs, we have shown that this positive MR at low fields is due to the reduction in the width of the canted spin structure around APBs and associated increase in the spin canting. This $DWMR_{APB}$ peaks at a particular temperature T_p and vanishes below T_V. We associate this with the difference between the spin-dependent transport mechanisms and hard-to-easy axis transition across T_V. We have also shown that $DWMR_{APB}$ depends on the size of the APB domains.

ACKNOWLEDGMENTS

This work was supported by the Science Foundation of Ireland (SFI) under contract no. 00/PI.1/C042.

APPENDIX: FOMRMATION OF APBs IN Fe_3O_4(110) FILMS GROWN ON MgO(110) SUBSTRATES

During the early stages of growth, adjacent Fe_3O_4 nucleation islands may be shifted by a $\sqrt{3/2}$ **a**⟨$\bar{1}$11⟩ or $\sqrt{3/2}$ **a**⟨$\bar{1}\bar{1}$1⟩ and a 1/2 **a** ⟨001⟩ shift vector. The islands separated by these shift vectors can eventually form APBs when they coalesce. Figures 10(a) and 10(b) show the possible APB formation with the boundary along ⟨001⟩ and ⟨$\bar{1}$10⟩directions. The direction of the boundary could be along other directions as well, not necessarily along ⟨001⟩ and ⟨$\bar{1}$10⟩. However, it is clear that shift vectors $\sqrt{3/2}$ **a**⟨$\bar{1}$11⟩ or $\sqrt{3/2}$ **a**⟨$\bar{1}\bar{1}$1⟩ lead predominantly to the formation of APB along low index direction ⟨001⟩ and likewise the shift vector 1/2 **a** ⟨001⟩ leads prominently to APB along a low index direction ⟨$\bar{1}$10⟩. Figures 10(b) and 10(c) show the possible antiferromangnetic and ferromagnetic superexchanges (SE) across APBs formed on the (110) and (100) surfaces.

*Corresponding author: sofins@tcd.ie

[1] A. D. Kent, J. Yu, U. Rudiger, and S. S. P. Parkin, J. Phys. Condens. Matter **13**, R461 (2001).
[2] C. H. Marrows, Adv. Phys. **54**, 585 (2005).
[3] P. M. Levy and S. Zhang, Phys. Rev. Lett. **79**, 5110 (1997).
[4] M. Viret, D. Vignoles, D. Cole, J. M. D. Coey, W. Allen, D. S. Daniel, and J. F. Gregg, Phys. Rev. B **53**, 8464 (1996).
[5] A. D. Kent, U. Rüdiger, J. Yu, L. Thomas, and S. S. P. Parkin, J. Appl. Phys. **85**, 5243 (1999).
[6] D. Ravelosona, A. Cebollada, F. Briones, C. Diaz-Paniagua, M. A. Hidalgo, and F. Batallan, Phys. Rev. B **59**, 4322 (1999).
[7] U. Ebels, A. Radulescu, Y. Henry, L. Piraux, and K. Ounadjela, Phys. Rev. Lett. **84**, 983 (2000).
[8] R. Danneau, P. Warin, J. P. Attané, I. Petej, C. Beigné, C. Fermon, O. Klein, A. Marty, F. Ott, Y. Samson, and M. Viret, Phys. Rev. Lett. **88**, 157201 (2002).
[9] R. F. Sabirianov, A. K. Solanki, J. D. Burton, S. S. Jaswal, and E. Y. Tsymbal, Phys. Rev. B **72**, 054443 (2005).
[10] L. Klein, Y. Kats, A. F. Marshall, J. W. Reiner, T. H. Geballe, M. R. Beasley, and A. Kapitulnik, Phys. Rev. Lett. **84**, 6090 (2000).
[11] S.K Arora, R. G. S. Sofin, I. V. Shvets, and M. Luysberg, J. Appl. Phys. **100**, 073908 (2006).

[12]M. Luysberg, R. G. S. Sofin, S. K. Arora, and I. V. Shvets, Phys. Rev. B **80**, 024111 (2009).
[13]I. Zutic, J. Fabian, and S. Das Sharma, Rev. Mod. Phys. **76**, 323 (2004).
[14]L. McGuigan, R. C. Barklie, R. G. S. Sofin, S. K. Arora, and I. V. Shvets, Phys. Rev. B **77**, 174424 (2008).
[15]M. Ziese, Rep. Prog. Phys. **65**, 143 (2002).
[16]S. K. Arora, Han-Chun Wu, R. J. Choudhary, I. V. Shvets, O. N. Mryasov, Hongzhi Yao, and W. Y. Ching, Phys. Rev. B **77**, 134443 (2008).
[17]S. Lee, A. Fursina, J. T. Mayo, C. T. Yavuz, V. L. Colvin, R. G. S. Sofin, I. V. Shvets and D. Natelson, Nat. Mater. **7**, 130 (2008).
[18]M. Ziese, A. Bollero, I. Panagiotopoulos, N. Moutis, Appl. Phys. Lett. **88**, 212502 (2006).
[19]R. Ramos, S. K. Arora, and I. V. Shvets, Phys. Rev. B **78**, 214402 (2008).
[20]Han-Chun Wu, Mohamed Abid, Byong S. Chun, Rafael Ramos, Oleg N. Mryasov, and Igor V. Shvets, Nano Lett. **10**, 1132 (2010).
[21]X. W. Li, A. Gupta, Gang Xiao, W. Qian, and V. P. Dravid, Appl. Phys. Lett. **73**, 3282 (1998).
[22]J. P. Hong, S. B. Lee, Y. W. Jung, J. H. Lee, K. S. Yoon, K. W. Kim, C. O. Kim, and C. H. Lee, Appl. Phys. Lett. **83**,1590 (2003).
[23]M. Ziese, Phys. Rev. B **62**, 1044 (2000).
[24]S. M. Watts, K. Nakajima, S. van Dijken, and J. M. D. Coey, J. Appl. Phys. **95**, 7465 (2004).
[25]S. Kale, S. M. Bhagat, S. E. Lofland, T. Scabarozi, S. B. Ogale, A. Orozco, S. R. Shinde, T. Venkatesan, B. Hannoyer, B. Mercey, and W. Prellier, Phys. Rev. B **64**, 205413 (2001).
[26]M. Zeise, R. Hohne, H. C. Semmelhack, H. Reckentin, N. H. Hong, and P. Esquinazi, Eur. Phys. J. B **28**, 415 (2002).
[27]D. Reisinger, M. Schonecke, T. Brenninger, M. Opel, A. Erb, L. Alff, and R. Gross, J. Appl. Phys. **94**, 1857 (2003).
[28]W. Eerenstein, T. T. M. Palstra, T. Hibma, and S. Celotto Phys. Rev. B **66**, 201101(R) (2002).
[29]A. V. Ramos, J.-B. Moussy, M.-J. Guittet, A. M. Bataille, M. Gautier-Soyer, M. Viret, C. Gatel, P. Bayle-Guillemaud, and E. Snoeck, J. Appl. Phys. **100**, 103902 (2006).
[30]J.-B. Moussy *et al.*, Phys. Rev. B **70**, 174448 (2004).
[31]S. K. Arora, R. G. S Sofin, and I.V. Shvets, Phys. Rev. B **72**, 134404 (2005).
[32]W. Eerenstein, T. T. M. Palstra, S. S. Saxena, and T. Hibma, Phys. Rev. Lett. **88**, 247204 (2002).
[33]D. T. Margulies, F. T. Parker, M. L. Rudee, F. E. Spada, J. N. Chapman, P. R. Aitchison, and A. E. Berkowitz, Phys. Rev. Lett. **79**, 5162 (1997).
[34]A. M. Bataille, L. Ponson, S. Gota, L. Barbier, D. Bonamy, M. Gautier-Soyer, C. Gatel, and E. Snoeck, Phys. Rev. B **74**, 155438 (2006).
[35]T. Kasama, R. E. Dunin-Borkowski, and W. Eerenstein, Phys. Rev. B **73**, 104432 (2006).
[36]Ricardo Aragón, Douglas J. Buttrey, John P. Shepherd, and Jurgen M. Honig, Phys. Rev. B **31**, 430 (1985).
[37]J. Orna, P. A. Algarabel, L. Morellón, J. A. Pardo, J. M. de Teresa, R. López Antón, F. Bartolomé, L. M. García, J. Bartolomé, J. C. Cezar, and A. Wildes, Phys. Rev. B **81**, 144420 (2010).
[38]M. Zeise and H. J. Blythe, J. Phys. Condens. Matter. **12**, 13 (2000).
[39]Q. Pan, T. G. Pokhil, and B. M. Moskowitz, J. Appl. Phys. **91**, 5945 (2002).
[40]C. A. Domenicali, Phys. Rev. **78**, 458 (1950).
[41]J. Feder, *Fractals* (Plenum, New York, 1988).
[42]D. Ihle and B Lorenz, J. Phys. C **18**, L647 (1985); D. Ihle and B. Lorenz, *ibid.* **19**, 5239 (1986).
[43]W. Eerenstein, T. T. M. Palstra, and T. Hibma, Thin Solid Films **400**, 90 (2001).